ISCI, Volume 7

Supplemental Information

Grafting Cobalt Diselenide on Defective Graphene for Enhanced Oxygen Evolution Reaction

Xin Wang, Linzhou Zhuang, Tianwei He, Yi Jia, Longzhou Zhang, Xuecheng Yan, Minrui Gao, Aijun Du, Zhonghua Zhu, Xiangdong Yao, and Shu-Hong Yu

Supplemental Information

Supplemental Figures

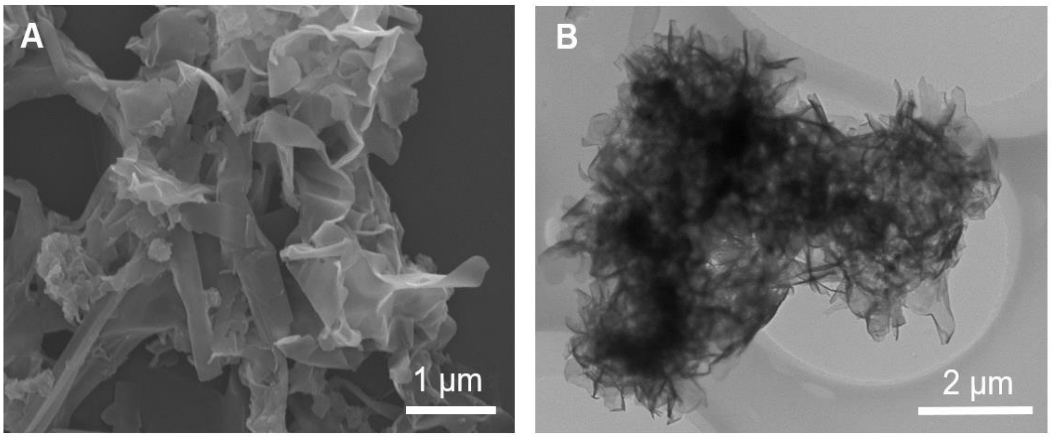

Figure S1. Characterization of $CoSe_2$/DETA hybrids, related to Figure 1.
SEM (A) and TEM (B) images of synthesized $CoSe_2$/DETA hybrids.

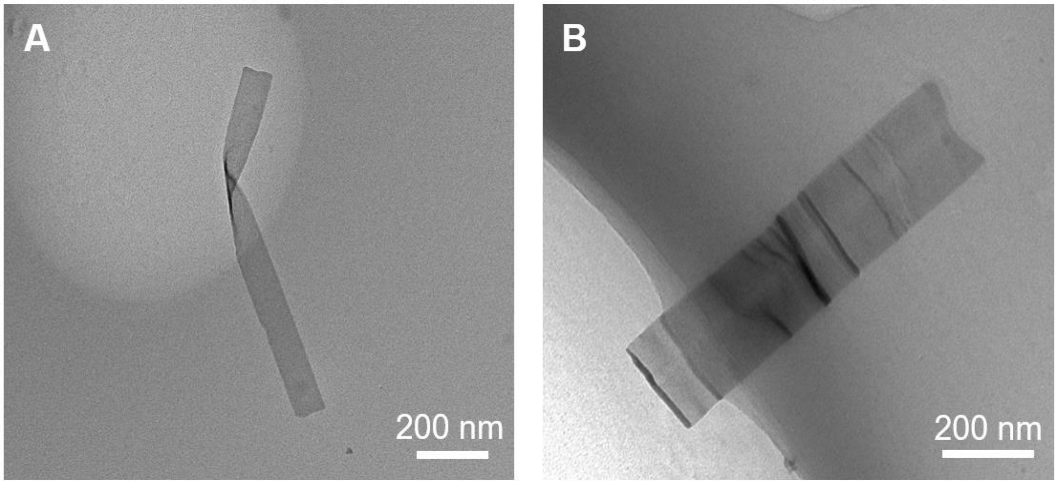

Figure S2. Characterization of exfoliated $CoSe_2$ ultrathin nanosheets, related to Figure 1.
TEM images of exfoliated $CoSe_2$ ultrathin nanosheets.

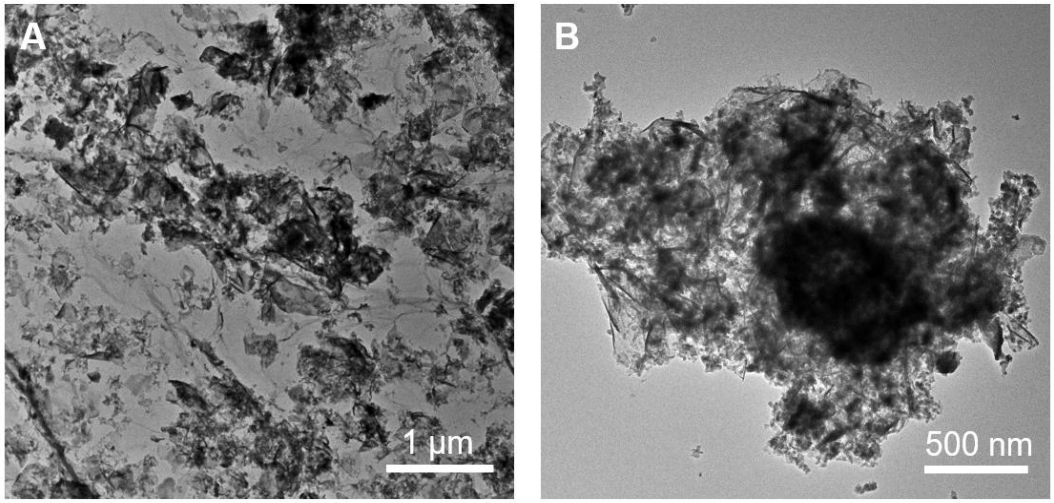

Figure S3. Characterization of different $CoSe_2$@DG samples, related to Figure 1.

TEM images of $CoSe_2$@DG samples prepared with the mass ratio of $CoSe_2$/DG as (A) 3:1 and (B) 6:1.

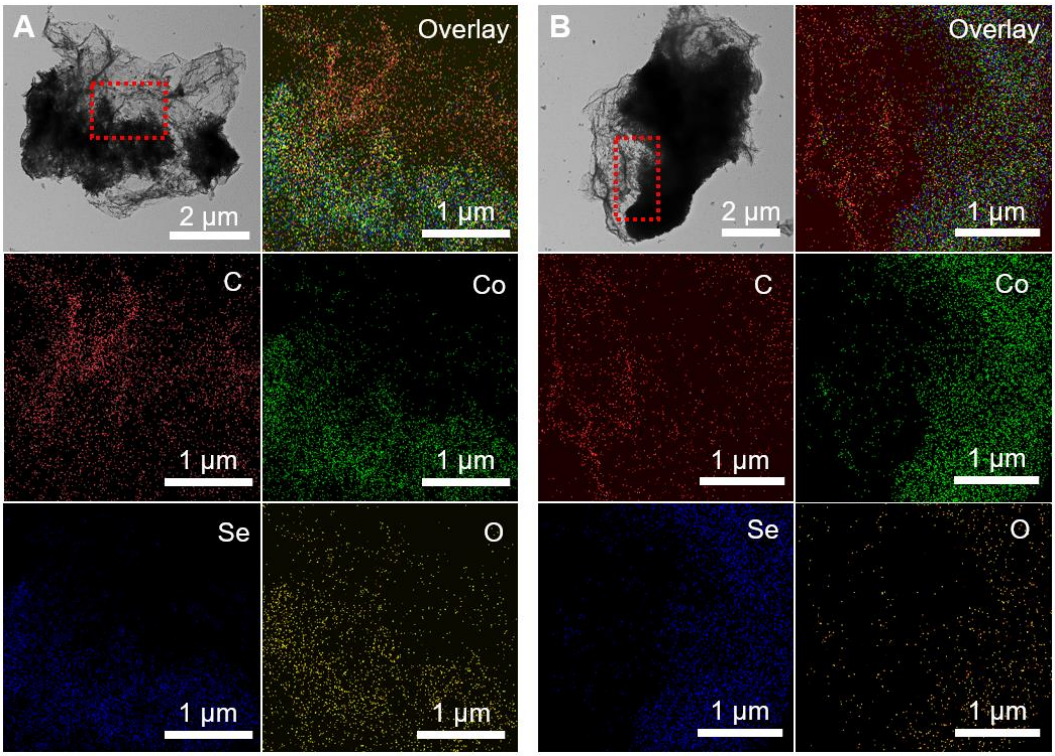

Figure S4. Characterization of $CoSe_2$@G and $CoSe_2$@NG composites, related to Figure 1.

STEM-EDS elemental mapping images of (A) $CoSe_2$@G and (B) $CoSe_2$@NG composites.

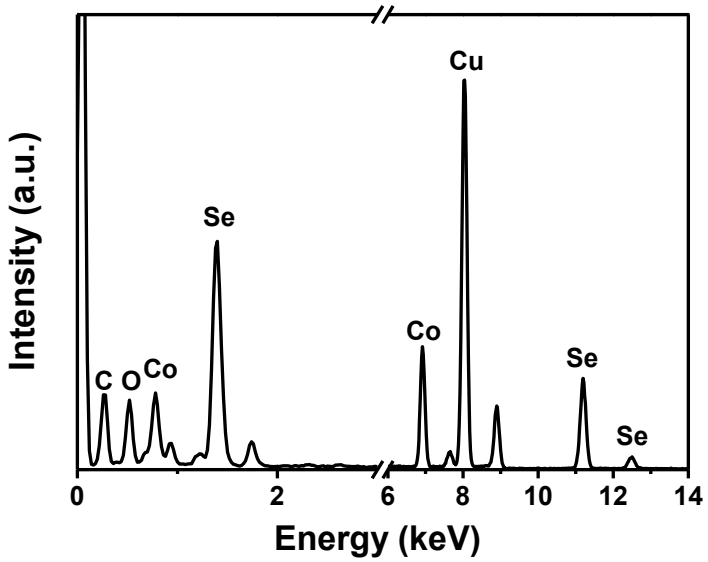

Figure S5. Characterization of $CoSe_2$@DG composites, related to Figure 1.
EDX spectrum of as-prepared $CoSe_2$@DG composites.

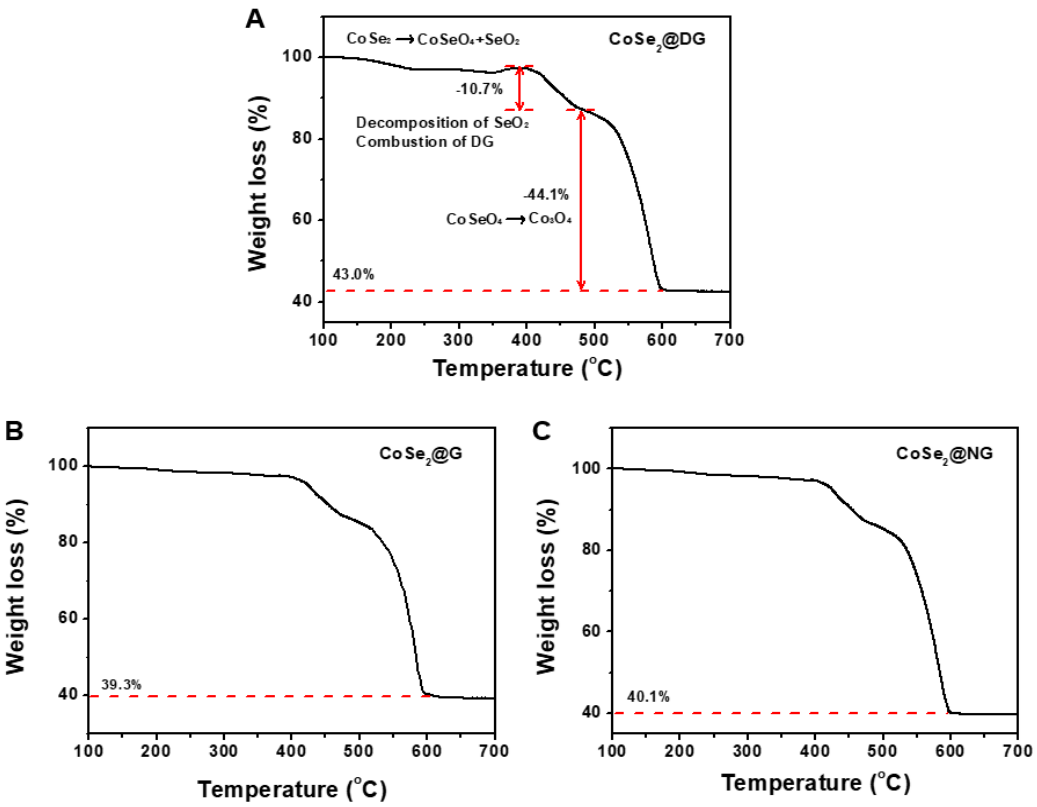

Figure S6. Characterization of $CoSe_2$@G, $CoSe_2$@NG, and $CoSe_2$@DG composites, related to Figure 1.

TGA curve of (A) $CoSe_2$@DG, (B) $CoSe_2$@G, (C) $CoSe_2$@NG composites under air atmosphere.

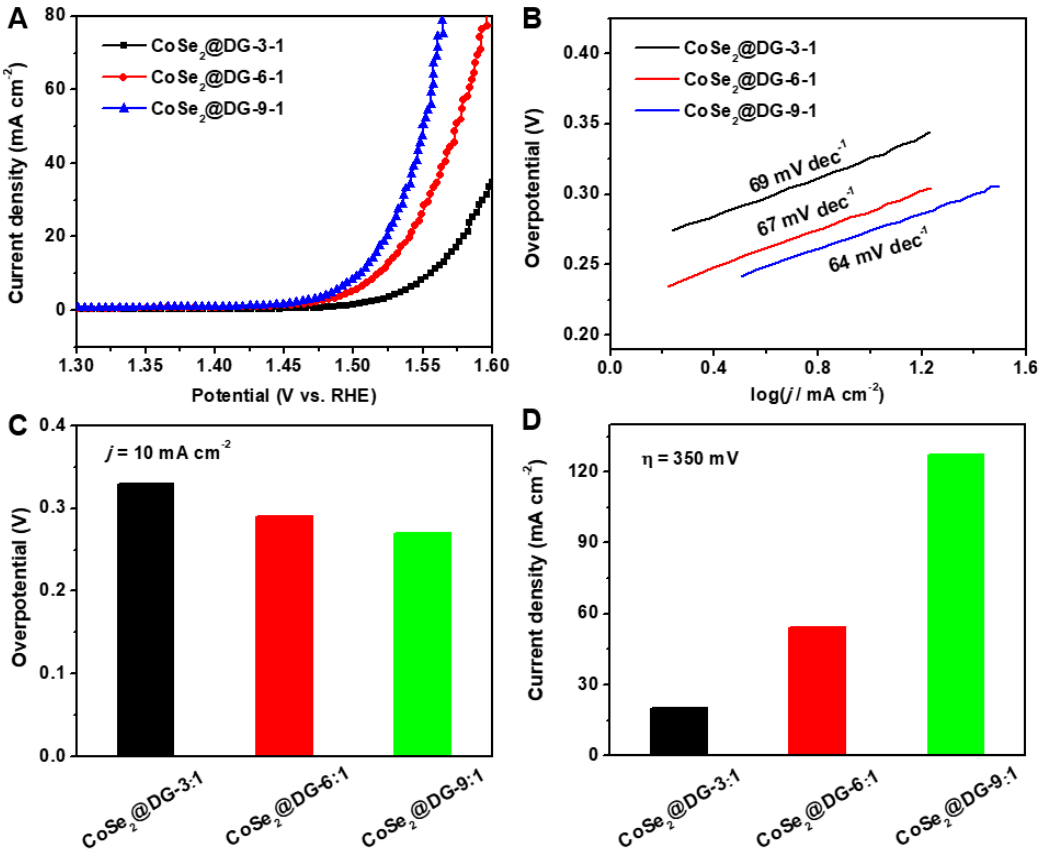

Figure S7. OER activity of $CoSe_2$@DG composites prepared with different mass ratio (3:1, 6:1, and 9:1), related to Figure 2.

(A) LSV curves, (B) Tafel plots, (C) Overpotential required for j=10 mA cm^{-2}, (D) Current densities at an overpotential of 350 mV.

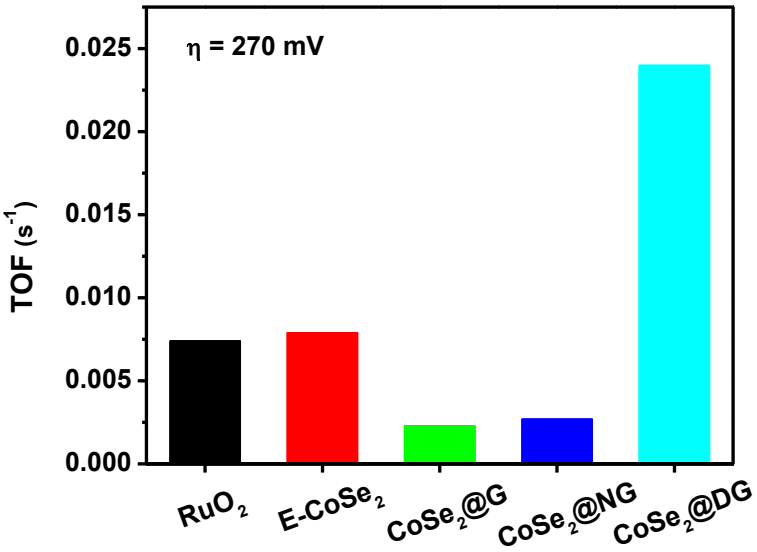

Figure S8. Intrinsic activity study of different catalysts, related to Figure 2.
Turnover frequency (TOF) of different catalysts at an overpotential of 270 mV.

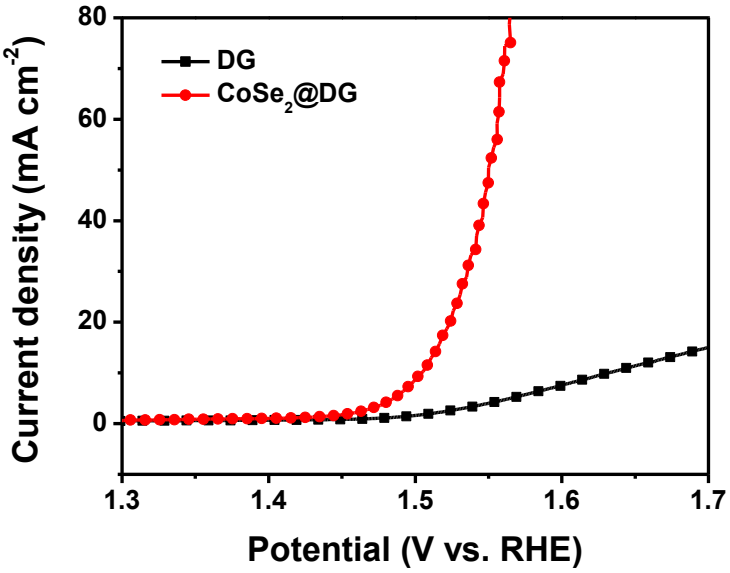

Figure S9. Comparison of OER activity between DG and $CoSe_2$@DG hybrid, related to Figure 2.
OER LSV curves of DG and $CoSe_2$@DG hybrid in 1 M KOH solution

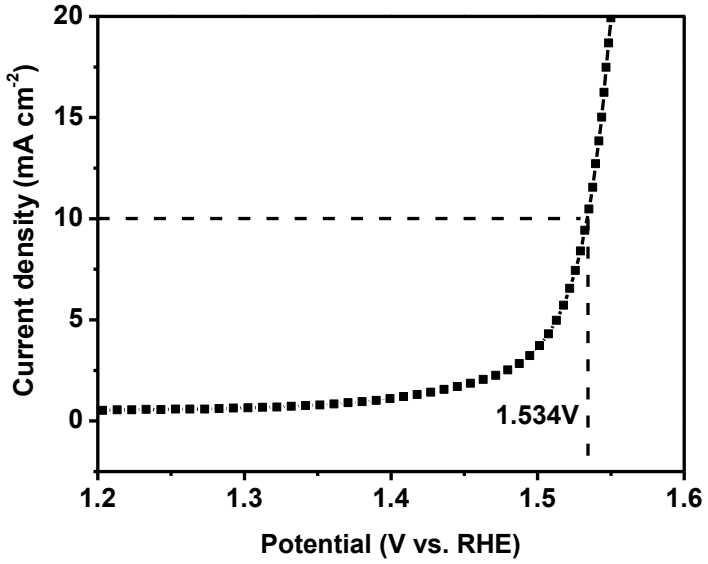

Figure S10. OER activity of $CoSe_2$@DG hybrid catalysts in 0.1 M KOH solution, related to Figure 2.
OER LSV curve of $CoSe_2$@DG hybrid catalysts in 0.1 M KOH solution.

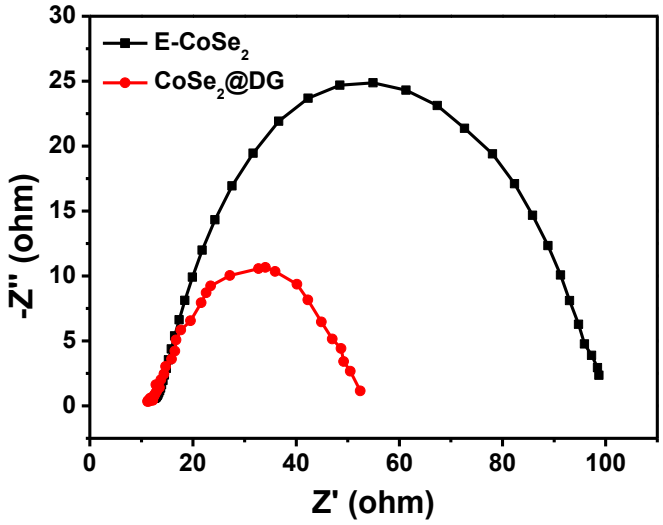

Figure S11. Impedance study of E-$CoSe_2$ and $CoSe_2$@DG, related to Figure 2.
Electrochemical impedance spectroscopy (EIS) Nyquist plots obtained at 1.33 V *vs.* RHE.

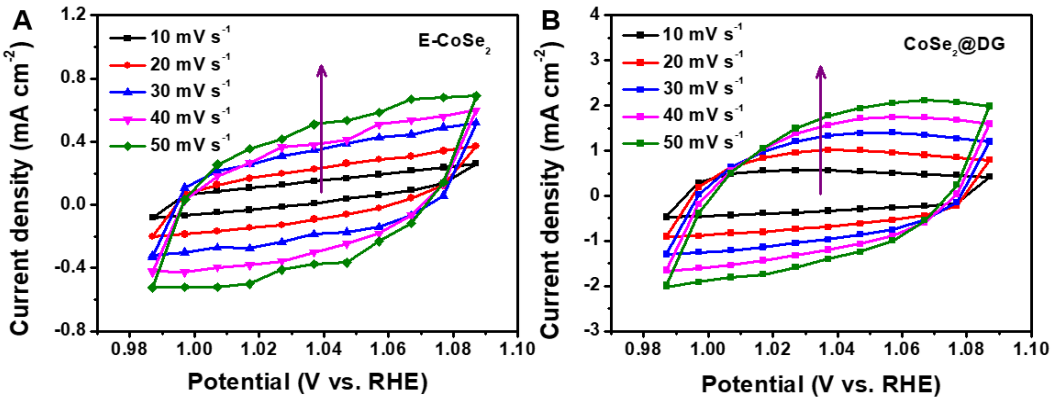

Figure S12. The electrochemical active surface areas (ECSAs) study of E-$CoSe_2$ and $CoSe_2$@DG catalysts, related to Figure 2.

Cyclic voltammetry curves of (A) E-$CoSe_2$ and (B) $CoSe_2$@DG catalysts at different scanning rate.

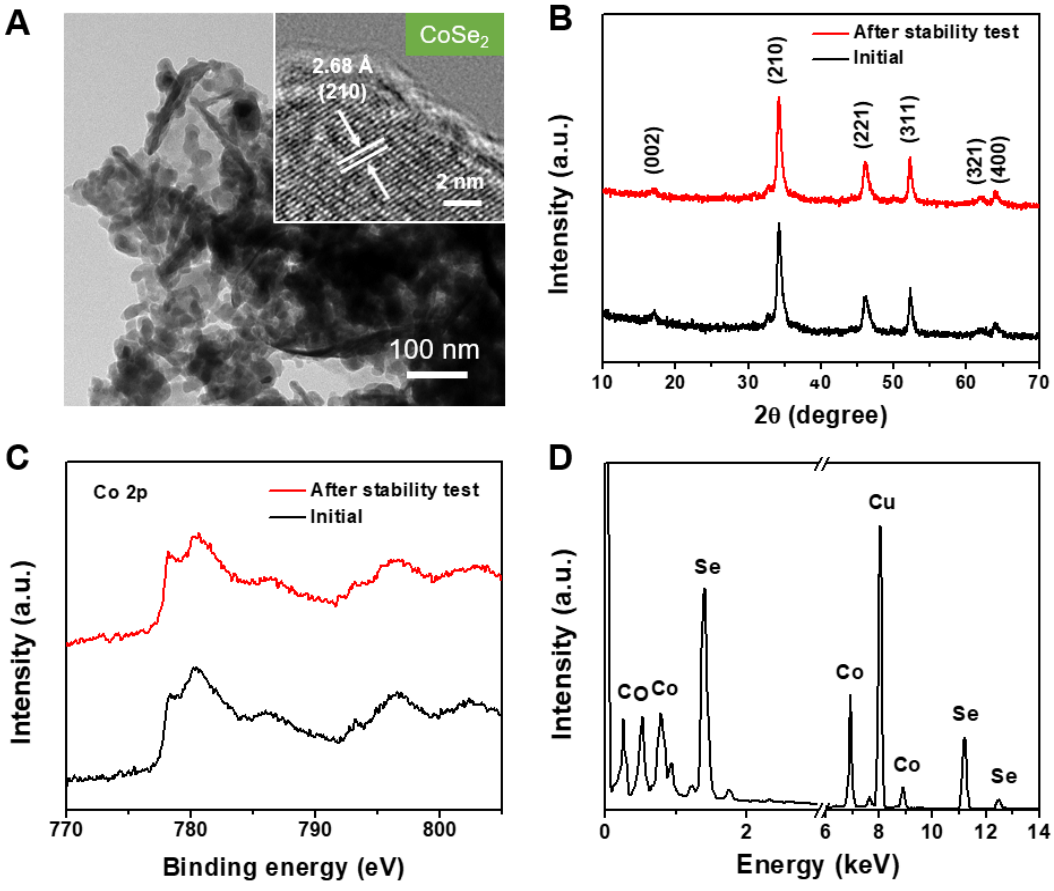

Figure S13. Characterization of $CoSe_2$@DG catalysts after continuous amperometric i-t measurement, related to Figure 2.

(A) TEM image, Inset: HRTEM image, (B) XRD patterns, (C) Co 2p XPS spectra, and (D) EDX spectrum.

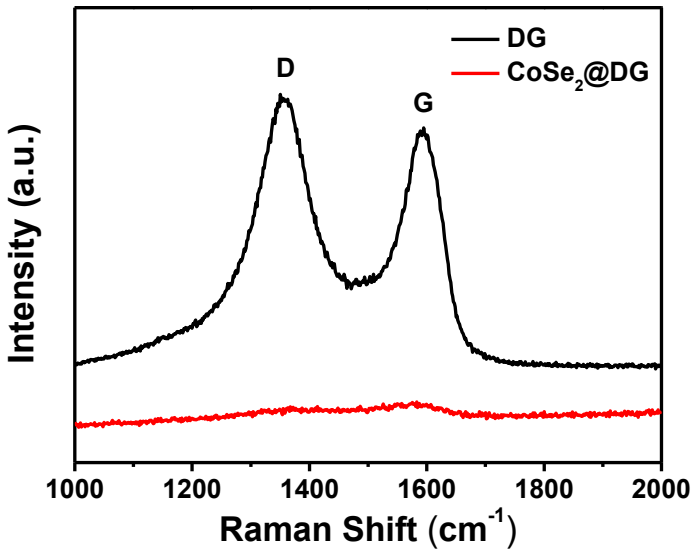

Figure S14. The study on the interaction between $CoSe_2$ and DG support, related to Figure 3.
Raman spectra of pure DG and as-prepared $CoSe_2$@DG composites.

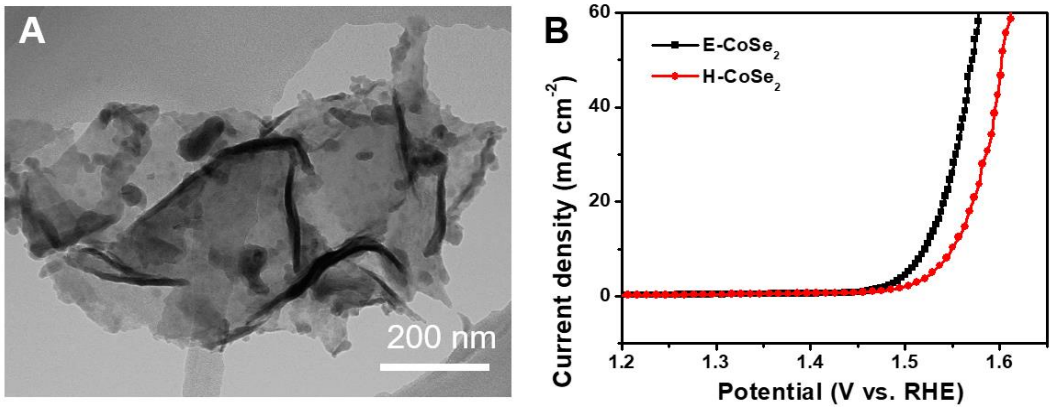

Figure S15. Characterization and OER activity of hydrothermal treated $CoSe_2$ (H-$CoSe_2$) without DG, related to Figure 3.
(A) TEM image of H-$CoSe_2$; (B) OER LSV curves of E-$CoSe_2$ and H-$CoSe_2$ samples.

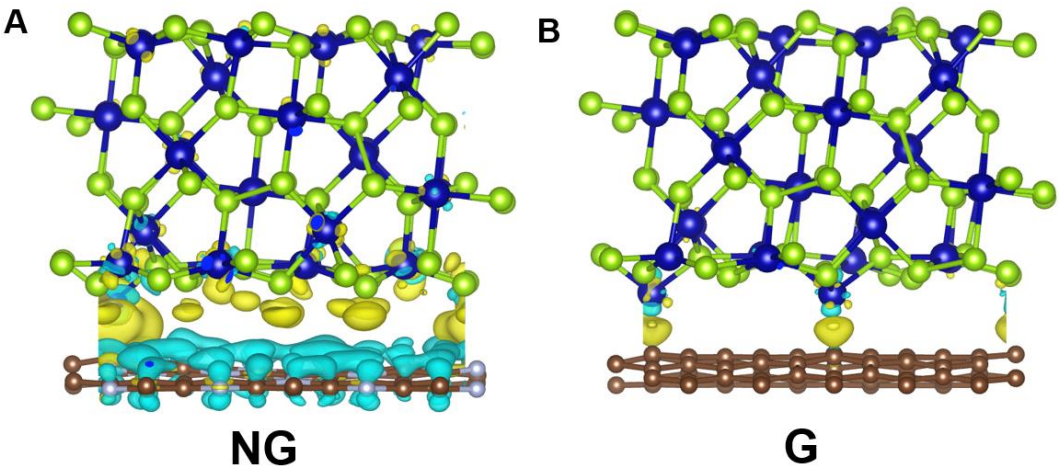

Figure S16. Charge density distribution of $CoSe_2$@NG and $CoSe_2$@G, related to Figure 4.
The side views of 3D charge density difference plot for the interfaces between graphene sheets (A for NG and B for G) and $CoSe_2$ layer calculated by DFT. Yellow and cyan isosurfaces represent charge accumulation and depletion in the 3D space with an isosurface value of 0.002 e $Å^{-3}$. Brown, green and blue balls represent C, Se and Co atoms, respectively.

Supplemental Table

Table S1. Electrocatalytic OER performance of our synthesized $CoSe_2$@DG hybrid catalysts compared with that of reported other non-precious metal electrocatalysts tested in alkaline solution, related to **Figure 2**.

Material	Electrolyte	η@10 mA cm^{-2} (mV)	*j*@350 mV (mA cm^{-2})	Tafel slope (mV dec^{-1})	Reference
$CoSe_2$@DG	**1M KOH 0.1M KOH**	**270 304**	**129 >20**	**64 N/A**	**This work**
$CoSe_2$ ultrathin nanosheets	0.1M KOH	320	<20	44	(Liu et al., 2014)
Metallic single-unit-cell $CoSe_2$ sheets	1M KOH	~340	<15	64	(Liang et al., 2015)
$CoSe_2$/CF	1M KOH	297	<50	41	(Sun et al., 2016)
$CoSe_2$/N-graphene	0.1M KOH	366	<10	40	(Gao et al., 2014)
CeO_2/$CoSe_2$	0.1M KOH	288	N/A	44	(Zheng et al., 2015)

Au nanoclusters/$CoSe_2$	0.1M KOH	410	<5	N/A	(Zhao et al., 2017)
Ag-$CoSe_2$	0.1M KOH	320	22.36	56	(Zhao et al., 2017)
$NiSe_2$ nanosheets	1M KOH	330	16.3	80	(Chen et al., 2017)
(Ni,Co)Se_2-GA	1M KOH	250	>100	70	(Xu et al., 2017)
$CoTe_2$	0.1M KOH	357	<20	32	(Gao et al., 2017)
N-doped CoS_2	1M KOH	240	~150	98	(Hao et al., 2017)
Fe-CoOOH/G	1M KOH	330	~30	37	(Han et al., 2017)
CoFe LDHs-Ar	1M KOH	266	N/A	37.85	(Wang et al., 2017)

Transparent Methods

Synthesis of $CoSe_2$-DETA lamellar nanohybrids

In a typical procedure, 2 mmol (0.498 g) of $Co(Ac)_2 \cdot H_2O$ was added into 26.0 mL of deionized water (DIW) under magnetic stirring. About 10 min later, 2 mmol (0.346 g) of Na_2SeO_3 and 52.0 mL of diethylenetriamine (DETA) were added. After stirring for 0.5 h in a beaker, the wine homogeneous solution was transferred into a 100 mL Teflon-lined autoclave, which was sealed and maintained at 180 ^oC for 16 h and then naturally cooled down to room temperature. The resulting solid product was collected and washed with absolute ethanol for 3 times to remove ions and possible remnants, and dried under vacuum at 60 ^oC for 16 h.

Exfoliation of $CoSe_2$-DETA lamellar nanohybrids

20 mg of $CoSe_2$-DETA product was dispersed in 40 mL of ethanol and then ultrasonicated in ice-water for 12 h. After ultrasonic treatment, the resultant dispersions were centrifuged at 9500 rpm for 10 min to remove the unexfoliated component. The supernatant is denoted as the exfoliated $CoSe_2$ nanosheet (E-$CoSe_2$) solution.

Synthesis of N doped graphene (NG) and defective graphene (DG)

Typically, the monolayer pristine graphene was mixed with melamine (mass ratio was 1:1), and annealed at 700 ^oC for 2 hours with a heating rate of 5 ^oC min^{-1} under nitrogen to prepare the NG. Before heating, two hours nitrogen gas flowing was needed to remove oxygen in the furnace tube. Then to prepare DG, NG was annealed at 1150 ^oC for 2 hours with a heating rate of 5 ^oC/min under nitrogen so as to subtract the nitrogen atom from the sample.

Synthesis of the $CoSe_2$@DG composite

Typically, a designed volume of DG, NG or G nanosheet (0.1 g L^{-1}) was added drop by drop into the exfoliated $CoSe_2$-NS solution under continuous stirring (the mass ratio of exfoliated $CoSe_2$ ultrathin

nanosheets and DG is 9:1). The solution was transferred into a 100 mL Teflon-lined autoclave, sealed and maintained at 60 °C for 12 h, and then naturally cooled to room temperature. The resulting product was separated by centrifugation.

Materials characterization

The samples were characterized by different analytic techniques. X-ray diffraction (XRD) patterns (2θ, 8-90°) were recorded on a Bruker D8-Advanced X-ray diffractometer using nickel-filtered Cu-Kα radiation. Electron microscope images were collected on a JEOL JSM-7001F scanning electron microscopy (SEM) at an acceleration voltage of 10 kV and a Tecnai 20 FEG transmission electron microscope (TEM) operated at 200 kV. X-ray photoelectron spectra were acquired on a Kratos Axis ULTRA X-ray photoelectron spectrometer (XPS) incorporating a 165 mm hemispherical electron energy analyser and a monochromatic Al Kα (1486.6 eV) radiation at 150 W (15 kV, 10 mA). The binding energies were determined using the C1s line at 284.6 eV from adventitious carbon as a reference. Raman spectra were recorded on a Renishaw InVia spectrometer using the 514 nm laser excitation. Thermogravimetric analysis (TGA) was carried out on a TA Instrument under air at a heating rate of 10 °C min^{-1}. The thickness of $CoSe_2$-NS was analysed by a Cypher (Asylum Research) atomic force microscope (AFM), whose cantilevers were HA_NC (Etalon) from NT-MDT, having a nominal spring constant of 4.5 N/m and nominal resonant frequency of 145 kHz. Before the AFM test the sample was dissolved in ethanol, centrifuged at 6000 rpm, and the liquid supernatant was diluted by 600 times, then dropped upon the mica plate.

Electrochemical measurements

All the electrochemical tests were performed in a conventional three-electrode system at an electrochemical station (Biologic VMP2/Z multichannel potentiostat), using Pt wire as counter electrode, glassy carbon electrode as working electrode, and an Ag/AgCl (3 M NaCl) electrode as reference electrode. For the preparation of $CoSe_2$ thin film electrode, 5 mg of catalyst powder was dispersed in 1 mL of 3:1 (v/v) DIW/2-propanol mixed solvent with 40 μL of Nafion solution (5 wt%), and then the mixture was ultrasonicated for about 1 h to generate a homogeneous ink. Next, 5.0 μL of the dispersion was transferred onto the glassy carbon disk, leading to the catalyst loading of 0.196 mg cm^{-2}. Finally, the as-prepared catalyst film was dried at room temperature. Linear sweep voltammetry (LSV) was performed at a continuous rotating speed of 1,600 rpm and a sweep rate of 5 mV/s. To assess the long-term electrocatalytic stability of $CoSe_2$@DG electrodes, the continuous amperometric i-t measurement was employed under a constant overpotential of 305 mV. The electrochemical impedance spectroscopy (EIS) measurement was carried out in the same configuration at room temperature with a sinusoidal voltage amplitude of 10 mV. The electrochemically active surface areas (ECSA) was determined by CV at the potential window 0.987 – 1.087 V (*vs.* RHE), with different scanning rate of 10, 20, 30, 40, and 50 mV/s. By plotting the difference between the anodic and cathodic current densities ($\Delta j = j_a - j_c$) at 1.037 V (*vs.* RHE) against the scan rates, the resulting linear slope is twice of the double layer capacitance (C_{dl}), which can be used to represent ECSA. The turnover frequency (TOF) value is calculated according to the following equation:

$$TOF = (J \times A) / (4 \times F \times n)$$

where J is the current density at a given overpotential (270 mV for our work), A is the surface area of the electrode (0.126 cm^2), the number of 4 represents 4 electrons/mol of O_2, F is the Faraday constant (96485.3 C/mol), and n stands for the number of moles of Co ions in as-made $CoSe_2$@DG, $CoSe_2$@G, $CoSe_2$@NG composites. In our case, all Co element was assumed to be catalytically active no matter whether they are

accessible to the electrolyte or not. Therefore, the calculated TOF value represents the lowest limit.

RHE calibration: In the all electrochemical tests, Ag/AgCl (3M NaCl) was used as the reference electrode. It was calibrated with regard to RHE. The calibration was performed in a H_2-saturated 1 M KOH electrolytes with a Pt-wire as the working electrode. CV curve was obtained at the scan rate of 1 mV s^{-1}, and the average potential at which the current crossed zero was regard as the thermodynamic potential for the hydrogen electrode reaction. The CV curve was shown as below:

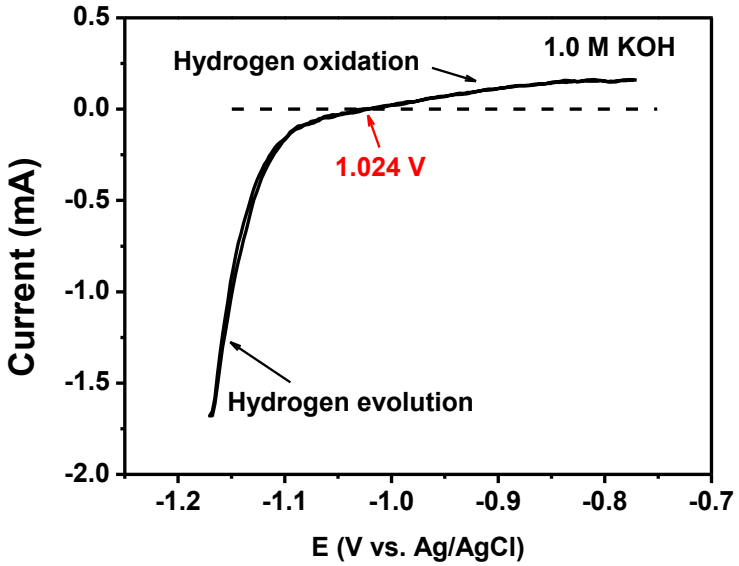

In 1 M KOH solution, all potentials were referenced to reversible hydrogen electrode (RHE) by following calculations: E (RHE) = E (Ag/AgCl) + 1.024 V.

Computational details

Density functional theory (DFT) as implemented in the Vienna Ab-initio Simulation Package (VASP) code were employed to perform the calculations (Kresse and Furthmüller, 1996a, 1996b). We use the generalized gradient approximation (Perdew et al., 1996) in the form of the Perdew–Burke–Ernzerhof functional (Perdew et al., 1996) to describe exchange-correlation interactions. Blöchl's all-electron, frozen-core projector augmented wave (PAW) method (Blöchl, 1994) was used to represent nuclei and core electrons. In all calculations, the van der Waals interaction was described by using the empirical correction in Grimme's scheme, i.e., DFT+D3 (Grimme, 2006). The Brillouin zone is sampled by gamma point. The electron wave functions were expanded using the plane waves with a cut off energy of 500 eV.

Supplemental References

Kresse, G., Furthmüller, (1996) Efficiency of ab-initio total energy calculations for metals and semiconductors using a plane-wave basis set. J., Comp. Mater. Sci. *6*, 15-50.

Kresse, G., Furthmüller, J., (1996) Efficient iterative schemes for *ab initio* total-energy calculations using a plane-wave basis set. Phys. Rev. B *54*, 11169.

Perdew, J. P., Burke, K., Ernzerhof, M., (1996) Generalized gradient approximation made simple. Phys.

Rev. Lett. *77*, 3865.

Perdew, J. P., Ernzerhof, M., Burke, K., (1996) Rationale for mixing exact exchange with density functional approximations. J. Chem. Phys. *105*, 9982-9985.

Blöchl, P. E., (1994) Projector augmented-wave method. Phys. Rev. B *50*, 17953.

Grimme, S., (2006) Semiempirical GGA-type density functional constructed with a long-range dispersion correction. J. Comput. Chem. *27*, 1787-1799.

Liu, Y., Cheng, H., Lyu, M., Fan, S., Liu, Q., Zhang, W., Zhi, Y., Wang, C., Xiao, C., Wei, S., Ye, B., Xie, Y., (2014) Low overpotential in vacancy-rich ultrathin $CoSe_2$ nanosheets for water oxidation. J. Am. Chem. Soc. 136, 15670-15675.

Liang, L., Cheng, H., Lei, F., Han, J., Gao, S., Wang, C., Sun, Y., Qamar, S., Wei, S., Xie, Y., Metallic single-unit-cell orthorhombic cobalt diselenide atomic layers: Robust water-electrolysis catalysts. Angew. Chem. Int. Ed. 54, 12004-12008.

Sun, C., Dong, Q., Yang, J., Dai, Z., Lin, J., Chen, P., Huang, W., Dong, X., (2016) Metal–organic framework derived $CoSe_2$ nanoparticles anchored on carbon fibers as bifunctional electrocatalysts for efficient overall water splitting Nano Research 9, 2234-2243.

Gao, M.-R., Cao, X., Gao, Q., Xu, Y.-F., Zheng, Y.-R., Jiang, J., Yu, S.-H., (2014) Nitrogen-doped graphene supported $CoSe_2$ nanobelt composite catalyst for efficient water oxidation. ACS Nano 8, 3970-3978.

Zheng, Y.-R., Gao, M.-R., Gao, Q., Li, H.-H., Xu, J., Wu, Z.-Y., Yu, S.-H., (2015) An efficient CeO_2/$CoSe_2$ nanobelt composite for electrochemical water oxidation. Small 11, 182-1888.

Zhao, S., Jin, R., Abroshan, H., Zeng, C., Zhang, H., House, S.D., Gottlieb, E., Kim, H.J., Yang, J.C., Jin, R., (2017) Gold nanoclusters promote electrocatalytic water oxidation at the nanocluster/$CoSe_2$ interface. J. Am. Chem. Soc. 139, 1077-1080.

Zhao, X., Zhang, H., Yan, Y., Cao, J., Li, X., Zhou, S., Peng, Z., Zeng, J., (2017) Engineering the electrical conductivity of lamellar silver-doped cobalt(ii) selenide nanobelts for enhanced oxygen evolution. Angew. Chem. Int. Ed. 56, 328-332.

Chen, S., Kang, Z., Hu, X., Zhang, X., Wang, H., Xie, J., Zheng, X., Yan, W., Pan, B., Xie, Y., (2017) Delocalized spin states in 2d atomic layers realizing enhanced electrocatalytic oxygen evolution. Adv. Mater. DOI: 10.1002/adma.201701687.

Xu, X., Liang, H., Ming, F., Qi, Z., Xie, Y., Wang, Z., (2017) Prussian blue analogues derived penroseite (Ni,Co)Se_2 nanocages anchored on 3D graphene aerogel for efficient water splitting. ACS Catal. 7, 6394-6399.

Gao, Q., Huang, C.-Q., Ju, Y.-M., Gao, M.-R., Liu, J.-W., An, D., Cui, C.-H., Zheng, Y.-R., Li, W.-X., Yu, S.-H.,(2017) Phase-selective syntheses of cobalt telluride nanofleeces for efficient oxygen evolution catalysts. Angew. Chem. Int. Ed. 27, 7877-7881.

Hao, J., Yang, W., Peng, Z., Zhang, C., Huang, Z., Shi, W., (2017) A nitrogen doping method for CoS_2 electrocatalysts with enhanced water oxidation performance. ACS Catal. 7, 4214-4220.

Han, X., Yu, C., Zhou, S., Zhao, C., Huang, H., Yang, J., Liu, Z., Zhao, J., Qiu, J., (2017) Ultrasensitive iron-triggered nanosized Fe-CoOOH integrated with graphene for highly efficient oxygen evolution. Adv. Energy Mater. DOI: 10.1002/aenm.201602148.

Wang, Y., Zhang, Y., Liu, Z., Xie, C., Feng, S., Liu, D., Shao, M., Wang, S., (2017) Layered double hydroxide nanosheets with multiple vacancies obtained by dry exfoliation as highly efficient oxygen

evolution electrocatalysts. Angew. Chem. Int. Ed. 27, 5961-5965.